Applied Physics B manuscript No.
(will be inserted by the editor)

Use of nonlinear properties of intracavity Type II Second Harmonic Generation for contrast enhancement, contour recognition and noise filtering in image processing

Adrian Jacobo[1], Pere Colet[1], Pierre Scotto[1], Maxi San Miguel[1]

Instituto Mediterraneo de Estudios Avanzados, IMEDEA (CSIC-UIB), Campus Universitat de les Illes Balears, E-07122 Palma de Mallorca, Spain

Received: date / Revised version: date

Abstract We discuss the use of intracavity type-II second harmonic generation for all-optical processing of images. Injecting an image in a pump beam linearly polarized and a homogeneous field in the orthogonally polarized pump it is possible to magnify the contrast and to recognize the contour of any part of the image whose intensity is above a tunable reference level. This can be done using ideal planar cavities where all the fields are resonant as well as in the more realistic situation where only the fundamental fields are resonant and using cavities with spherical mirrors.
PACS:42.30.-d, 42.65.Ky, 42.65.Pc

1 Introduction

Various techniques for image processing have been available in the last decades [1]. These techniques require first the detection of the optical image by means of a two dimensional array of photodetectors. In a second step, the digital version of the image is processed numerically. While this has proven to be quite flexible approach offering many possibilities, there is still a real interest in developing all-optical image processing schemes. In this schemes the detection of the image is avoided, reducing the errors due to an imperfect calibration of the individual photodetectors, as well as the noise added by the measurement process and subsequent electronic transmission. These effects, which deteriorate the quality of the image before processing, are, in the all optical case, absent or postponed to the very end of the information processing chain. Secondly, the maximal resolution achievable, which is in digital image processing limited by the density of pixels in the detection plane, is set, in an all-optical scheme, only by diffraction. Finally, an all-optical scheme takes advantage of parallelism, which is a specific feature of optics. All-optical image processing operations that have been demonstrated include frequency transfer of an optical image from the infrared to the visible domain [2,3], and from the visible to the UV domain [4,5], as well as parametric amplification of an UV image [6,7], and contrast inversion [8]. In these schemes, an optical image at a frequency ω is directly injected into a nonlinear (NL) crystal illuminated with a strong monochromatic pump wave at frequency ω_p and the processed image is formed in the output plane. As a result of the nonlinearity of the crystal, the input image will be, depending on some phase matching condition, either transferred to a higher frequency $\omega + \omega_p$ by simple frequency addition [2–4], or amplified by photon down conversion [6–8]. In the latter case the amplification is accompanied by the formation of a phase conjugated (idler) image at the complementary frequency $\omega_p - \omega$. Considering the spatial dependence of the image processing mechanism on the position of the object in the transverse plane, the phase matching condition will determine whether image processing will be efficient either on a disk centered on the optical main axis of the system, or on a ring of finite width. This latter regime is also useful for selectively amplifying some Fourier components of a given image, leading to contrast enhancement or inversion.

Recently the use of nonlinear crystals inside a optical cavity rather in a propagation configuration has been proposed. The fundamental difference is the existence of instability thresholds which, if used appropriately, allow for a nonlinear processing of the image. For example, considering type-II second harmonic generation inside an ideal planar cavity where all the fields are resonant, it has been shown that it is possible to selectively enhance the contrast of part of an image or to detect its contour [9]. While this may be considered as a first prove of principle, triple resonant planar cavities are quite unsuitable for practical applications. Cavities where only the fundamental field is resonant or with spherical mirrors are by far more easy to stabilize and operate. We consider here the second harmonic generation inside these cavities

and study its possible applications for all-optical image processing.

The paper is organized as follows. In section 2 we introduce our theoretical model. Section 3 is devoted to the case of Fabry Perot cavities with plane mirrors. We review results obtained for triple resonant cavities [9]. In section 4 we address the case of non resonant second harmonic field. Section 5 is devoted to the case of cavities with spherical mirrors. We summarize our results in section 6.

2 The model

We consider a $\chi^{(2)}$ nonlinear crystal placed inside an optical cavity. Assuming a type II phase matching, a second harmonic field will be generated if the cavity is pumped by two orthogonally lineal polarized fields E_x and E_y. This system can be described by a set of equations similar to those used in [10] for an optical parametric oscillator:

$$\begin{aligned}
\partial_t B(r,\phi,t) &= -(k_B + \imath\delta_B - \imath\xi L_B)B(r,\phi,t) \\
&\quad -\chi A_x(r,\phi,t)A_y(r,\phi,t) \\
\partial_t A_x(r,\phi,t) &= -(k_A + \imath\delta_A - \imath\xi L_A)A_x(r,\phi,t) \\
&\quad +\chi A_y^*(r,\phi,t)B(r,\phi,t) + E_x(r,\phi,t) \\
\partial_t A_y(r,\phi,t) &= -(k_A + \imath\delta_A - \imath\xi L_A)A_y(r,\phi,t) \\
&\quad +\chi A_x^*(r,\phi,t)B(r,\phi,t) + E_y(r,\phi,t)
\end{aligned} \tag{1}$$

where the longitudinal dependence of the fields is eliminated using the paraxial and the mean field approximations [11]. The transverse variables r and ϕ denote the distance from the axis of the system and the angular variable, respectively. A_x and A_y are the linearly polarized intracavity field envelopes with fundamental frequency ω_A and B is the second harmonic field envelope at frequency $\omega_B = 2\omega_A$. χ is the nonlinear coupling strength, ξ is the effective transverse mode spacing, k_A and k_B are cavity linewidths for the fundamental and second harmonic fields and δ_A and δ_B are the respective detunings.

The effect of diffraction and the geometry of the cavity are taken in account by the differential operator

$$L_k = \frac{W_k^2}{4}\nabla_\perp^2 - \frac{r^2}{W_k^2} + 1\,, \qquad k = A, B \tag{2}$$

where $W_k = \sqrt{(2z_r c)/\omega_k}$ is the minimum waist of the intracavity fields, z_r is the common Rayleigh length of the three fields, c the speed of the light and $\nabla_\perp$ the transverse Laplacian. The first term of Eq. 2 models diffraction in the paraxial approximation while the r^2 term comes from the curvature of the mirror.

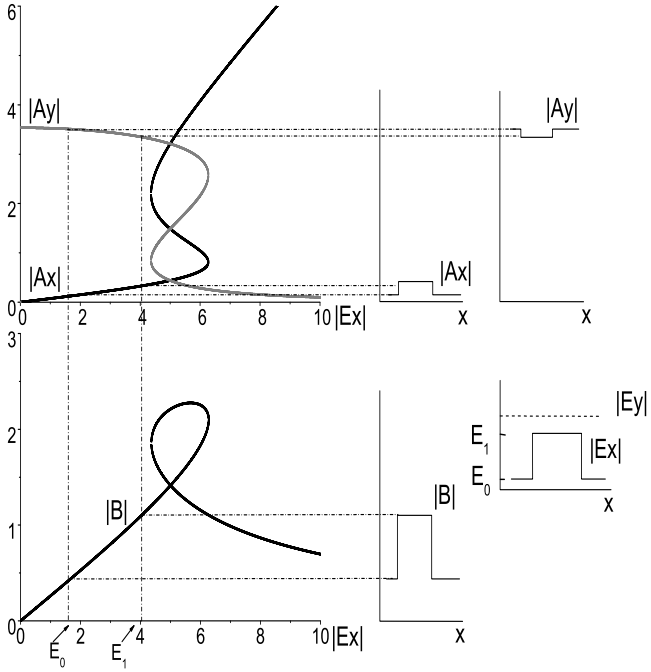

Fig. 1 Steady states for second harmonic generation with asymmetric homogeneous pumping and the geometrical construction to illustrate the frequency transfer regime. On the left we plot the stationary amplitude of the intracavity fields for homogeneous asymmetric pumping as a function of $|E_x|$ for $|E_y| = 5$ ($\delta_B = 0$, and $\delta_A = 1$). On the right we plot the response of the system to a simple image (sketched on the far right) where $|E_x|$ takes only the values E_0 and E_1 with $E_0 < E_1 < |E_y|$.

3 Image processing in a planar cavity

We now consider the case in which $\xi \to 0$ while $W_k \to \infty$ in such a way that the product ξW_k^2 converges to a finite value. The diffraction term in Eq.2 remains finite while the term associated with the mirror's curvature term vanishes; so that case corresponds to an ideal planar cavity. Rescaling $\chi A_x \to A_x$, $\chi A_y \to A_y$, $\chi B \to B$, $\chi E_x \to E_x$, $\chi E_y \to E_y$ and $\frac{\xi W_A^2}{4}\nabla_T^2 \to \nabla_T^2$; and taking $k_A = k_B = 1$ we recover the model for a planar cavity [12–15]

$$\partial_t B = -(1 + \imath\delta_B)B + \frac{\imath}{2}\nabla_\perp^2 B + \imath A_x A_y \tag{3}$$

$$\partial_t A_x = -(1 + \imath\delta_A)A_x + \imath\nabla_\perp^2 A_x - \imath A_y^* B + E_x \tag{4}$$

$$\partial_t A_y = -(1 + \imath\delta_A)A_y + \imath\nabla_\perp^2 A_y - \imath A_x^* B + E_y \tag{5}$$

For pumps homogeneous in the transverse plane, E_x and E_y can be taken as real fields without loss of generality. Typically, Eqs. [3]-[5] have been considered for the case of symmetrical pumping $E_x = E_y$, which maximizes the production of second harmonic. In such case the homogeneous stationary steady state shows a polarization instability for a pump above the critical value [12–16]:

$$E_{as}^2 = 2(1+\delta_B^2)^{1/2}(1+\delta_A^2)^{3/2} + 2(1+\delta_A^2)(1-\delta_A\delta_B).$$

For asymmetric homogeneous pumping $E_x \neq E_y$ the homogeneous steady state for $|A_y|$ is given by the solution of the polynomial

$$\begin{aligned}&\Delta_A|A_y|^{10} + [4(1-\delta_b)\Delta_A - |E_y|^2]|A_y|^8 + \\ &2[\Delta_A Q + \Delta_{AB}(|E_x|^2 - 2|E_y|^2)]|A_y|^6 \\ &+2\{2\Delta_A^2\Delta_B^2\Delta_{AB} - Q|E_y|^2 - 2\Delta_{AB}^2|E_x|^2\}|A_y|^4 \\ &+[\Delta_A^3\Delta_B^2 + 2\Delta_A\Delta_B\Delta_{AB}(|E_x|^2 - 2|E_y|^2)]|A_y|^2 \\ &-\Delta_A^2\Delta_B^2|E_y|^2 = 0. \end{aligned} \quad (6)$$

where $\Delta_A = 1+\delta_A^2$, $\Delta_B = 1+\delta_B^2$, $\Delta_{AB} = 1-\delta_A\delta_B$ and $Q = (\delta_A+\delta_B)^2 + 3\Delta_{AB}^2$. Once $|A_y|$ is known, $|A_x|$ and $|B|$ are given by

$$\begin{aligned}|A_x|^2 &= \frac{\Delta_B|E_x|^2}{|A_y|^2 + 2\Delta_{AB}|A_y| + \Delta_A\Delta_B} \\ |B|^2 &= \frac{|A_x|^2|A_y|^2}{\Delta_B} \end{aligned} \quad (7)$$

Fig.1 shows the typical dependence of the stationary solutions for the intracavity fields $|A_x|$, $|A_y|$ and $|B|$ on E_x when E_y is fixed to a given value, in this case $E_y = 5$. For small E_x, the functions $A_x(E_x)$ and $B(E_x)$ take small values while $A_y(E_x)$ is large and close to $E_y/(1+i\delta_A)$. All of them are single valued. When E_x approaches E_y the system displays bistability. $A_x(E_x)$ and $A_y(E_x)$ become S shaped and $B(E_x)$ closes over itself. For large E_x all the functions become again single valued but now $A_x(E_x) \gg A_y(E_x)$. The existence of three steady-state solutions of Eqs. 3-5 in a region of finite width centered on $E_x = E_y$ is closely related to the polarization instability occurring in the symmetrical pumping case. If fact,this S shape can be observed only if $E_y > E_{as}$

In the following we consider the effects produced on an image inserted in the system as spatial variations in the intensity of the x-polarized pump field along with an homogeneous pump E_y. Tuning the amplitude of the homogeneous pump it is possible to achieve different regimes of operation. In a first regime the image can be transferred from the fundamental to the second harmonic. In a second regime it is possible to enhance its contrast and to detect the contour of the image [9]. Furthermore, it is also possible to filter noise eventually present in the image.

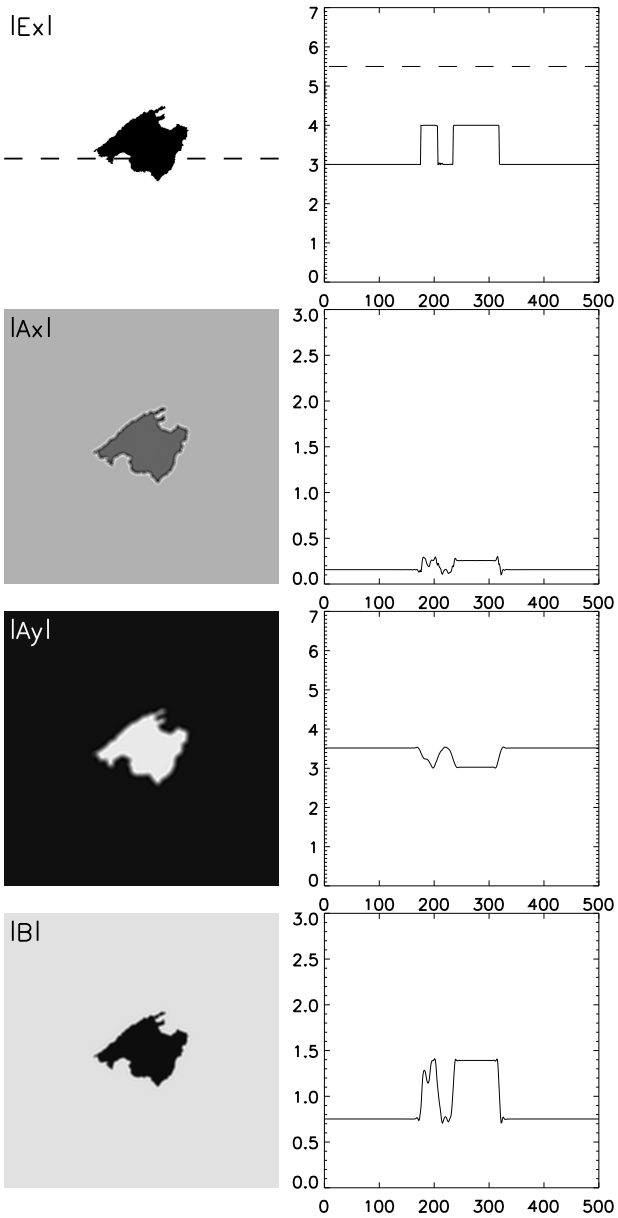

Fig. 2 Frequency transfer. The left column shows (from top to bottom) the spatial distribution of amplitude of the input image $|E_x|$, and the amplitude of the intracavity fields $|A_x|$, $|A_y|$ and $|B|$. The gray scale of goes from the minimum (white) to the maximum (black) of each field. The right column shows a transversal cut of the fields along the dashed line on the top left panel. We have considered $E_y = 5$ (shown as dashed line on the top right panel).

3.1 Frequency transfer

We consider the injection of a very simple 1-dimensional image in which the amplitude of the x-polarized signal $|E_x(x)|$ takes only two real values E_0 and E_1 along the transverse coordinate x, as shown in Fig. 1($|E_y| > E_1 > E_0$). At each spatial point the intracavity fields $A_{x,y}(x)$ and $B(x)$ tend to take the stationary values shown in Fig.1 corresponding to homogeneous pumps of amplitude E_0 and E_1, despite the spatial coupling caused by diffraction. This coupling becomes relevant for image details on the scale of the diffraction length. As sketched in Fig. 1, if $|E_x|$ remains well below $|E_y|$, A_x never leaves the lower branch of the curve $A_x(|E_x|)$, so A_x reproduces the spatial distribution of the input image $|E_x|$. The y-polarized intracavity field A_y shows the negative of the image. More important, the second harmonic field B reproduces $|E_x|$, so the image in the fundamental field is transferred to the second harmonic. As the image is

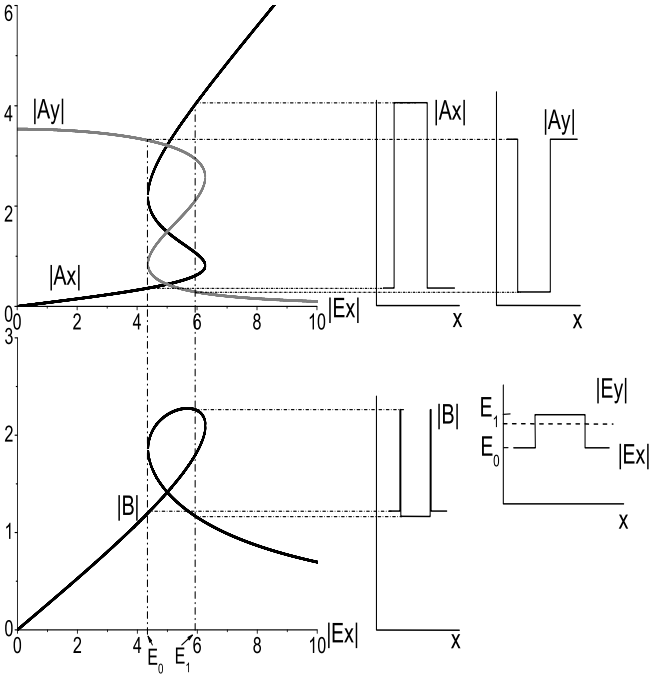

Fig. 3 Geometrical construction to illustrate the contrast enhancement and contour recognition regime. On the left we plot the stationary amplitude of the intracavity fields for homogeneous asymmetric pumping as a function of $|E_x|$ for $|E_y = 5|$. On the right we plot the response of the system to a simple image (sketched on the far right) where $|E_x|$ takes only the values E_0 and E_1 with $E_0 < |E_y| < E_1$.

encoded in the x-polarized fundamental field and B is y-polarized, there is simultaneously a transfer in the polarization of the image. These effects are shown in a more realistic 2d-image in Fig. 2 where an image of constant amplitude 1 is put on top of a plane wave background with amplitude $E_x = 3$. In this image can be seen that as an effect of the diffraction the edges of the image are soften. The image in the intracavity and second harmonic fields can be considered as the union of two different stationary states and the oscillatory tails of the front connecting the two states induce some distortion near the border. Nevertheless the image is quite well reproduced as seen in Fig.2.

3.2 Contrast enhancement and contour recognition

Let us consider again the simple 1-d image where $|E_x|$ takes only two values E_0 and E_1 along the transverse coordinate but now the lower value E_0 is below E_y while the higher value E_1 is above, as shown in Fig.3 ($E_1 > E_0 > |E_y|$). In this case the multivalued dependence of $A_x(|E_x|)$, $A_y(|E_x|)$ and $B(|E_x|)$ comes into play. If E_1 is larger than the upper end of the hysteresis cycle and E_0 is smaller than the lower end, $A_x(|E_x(x)|)$ has to jump from the lower to the upper branch, while $A_y(|E_x(x)|)$ has to jump from the upper to the lower branch. This will give rise to a sharp spatial variation of A_x and A_y. In

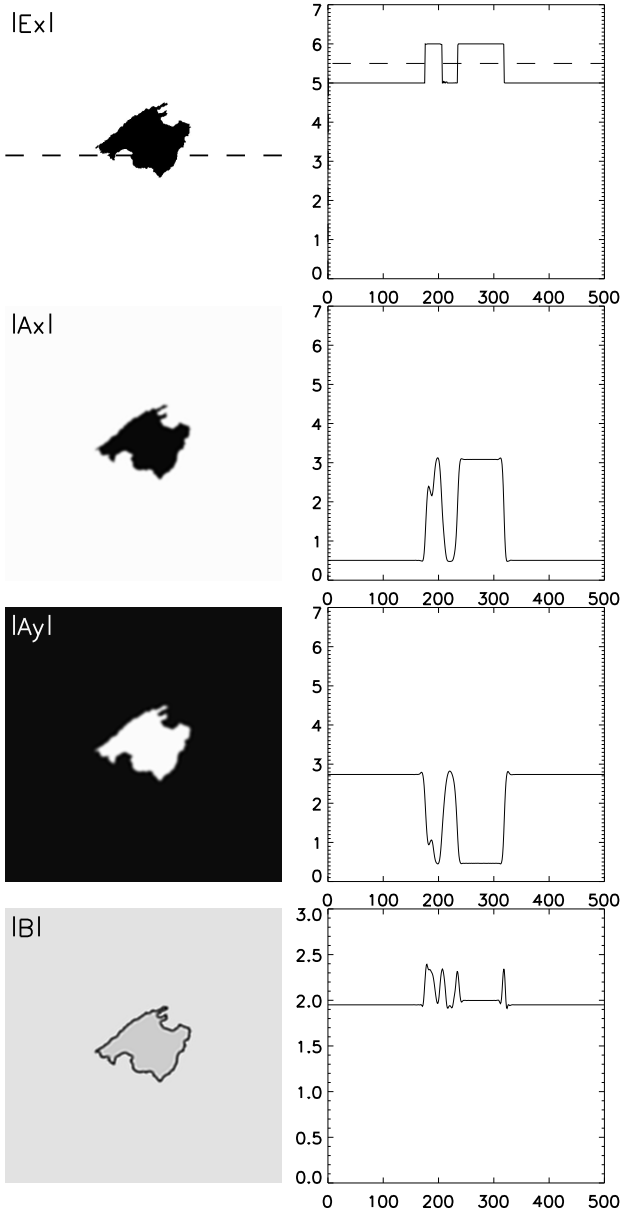

Fig. 4 Contrast enhancement and contour recognition. The left column shows (from top to bottom) the spatial distribution of amplitude of the input image $|E_x|$, and the amplitude of the intracavity fields $|A_x|$, $|A_y|$ and $|B|$. The gray scale of goes from the minimum (white) to the maximum (black) of each field. The right column shows a transversal cut of the fields. We have considered $|E_y| = 5$.

fact for vanishing intracavity fields as initial condition, it is not necessary to fully cross the hysteresis cycle to have a jump. With those initial conditions where $|E_x| < |E_y|$ the system locally selects the steady state solution with small value for $|A_x|$ and a large value for $|A_y|$, while it selects the steady state solution with a large value for $|A_x|$ and a small value for $|A_y|$ where $|E_x| > |E_y|$. Therefore, the reference value $|E_y|$ plays in fact the role of an effective threshold and the jump already occurs if $|E_x|$ crosses $|E_y|$ as sketched in Fig.3. In the region where $|E_x(x)|$ is

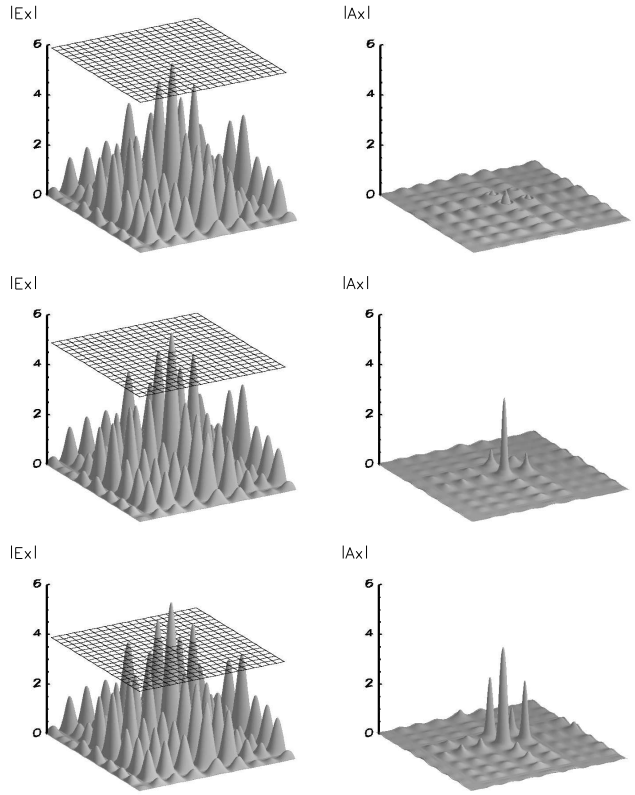

Fig. 5 Scanning of a 2 dimensional gray scale image. The left column shows the input image $|E_x(r,\phi)|$ and the homogeneous reference level $|E_y|$ plotted as a regular grid. The right column shows the amplitude of the x-polarized fundamental intracavity field $A_x(r,\phi)$ From top to bottom $|E_y|$ takes the values 6, 5 and 4.

larger than the reference level $|E_y|$, $|A_x|$ has a large value compared with the zones where $|E_x(x)| < |E_y|$; so the contrast in this field appears enhanced with respect to the contrast in the input fields (Fig.3). The amplitude $|A_y|$ takes lower values where $|E_x| < |E_y|$ leading to an image which is inverted with respect to the input (Fig.3). At the crossing points $|E_x| = |E_y|$ the second harmonic field B displays a sharp peak, since locally $|A_x| \simeq |A_y|$; i.e. the system goes trough the symmetric steady-sate solution characterized by a higher intracavity second harmonic field than the asymmetric stable ones. As a consequence the second harmonic field displays the contour of the input image Fig.3. The effects are shown for two dimensional case in Fig.4 where the last row shows the contour recognition. Image processing is slightly affected by diffraction effects in two dimensions, which tends to smooth out sharp angles in the input image and sets a minimum contrast below which no contrast enhancement can occur.

It should be emphasized that the previous results show that for a given image different processing capabilities are possible tuning the amplitude of the homogeneous field $|E_y|$. This is even more interesting when considering images which are composed of many levels of intensity, as in a gray scale image. In that sense, if the homogeneous pump $|E_y|$ is set to a value larger than $|E_x(r,\phi)|$ for any r and ϕ then the frequency transfer process will take place and the whole image will be displayed by the second harmonic frequency field $B(r,\phi)$. If $|E_y|$ is decreased, then the parts of the image where $|E_x(r,\phi)| > |E_y|$ will undergo a contrast enhancement process. As illustrated in Fig.5 for a 2-dimensional image the intracavity field $|A_x|$ is largely enhanced in these spatial regions. Simultaneously the amplitude of the second harmonic field $|B|$ shows the contour of the region whose contrast has been enhanced. The amplitude of the homogeneous pump acts as a tunable reference level and placing it at different values allows for the selective enhancement (and selective contour detection) of different parts of the figure (see Fig.5)

3.3 Noise filtering

Another interesting effect arises when the image inserted is superimposed with a random field, creating a noisy image. In this case the system shows noise filtering properties, and the images at the fundamental and second harmonic fields have a lower noise level than the input image. The noise filtering effect arises as an interplay between the diffraction and the nonlinear interaction [9]. It appears both in the frequency transfer regime and in the contour recognition regime but it is more effective in the second case, when the nonlinearities play a more important role and the contrast of the image is enhanced, as can be seen from Figs. 6 and 7.

4 Single resonant planar cavities

We next consider the casein which the second harmonic field is not resonant with the natural frequency of the cavity as it is often the case in practical situations. We do this by adiabatically eliminating the second harmonic variable B, $B = \imath A_x A_y/(1+\imath\delta_B)$ so the Eqs.(3), (5) and (4) become

$$\partial_t A_x = -(1+\imath\delta_A)A_x + \imath\nabla_T^2 A_x + \frac{|A_y|^2 A_x}{1+\imath\delta_B} + E_x \quad (8)$$

$$\partial_t A_y = -(1+\imath\delta_A)A_y + \imath\nabla_T^2 A_y + \frac{|A_x|^2 A_y}{1+\imath\delta_B} + E_y \quad (9)$$

The steady state homogeneous solutions remain the same, so that the previous discussion remains valid. In particular, contrast enhancement can be performed as before if the input image $|E_x|$ crosses the reference level $|E_y|$ as shown in Fig. 8 for a 2-dimensional noisy image processed by numerical integration of Eqs.(8) and (9). The noise-filtering properties are still present in this case. Furthermore, the contour recognition operation can also be performed by measuring the product $|A_x||A_y|$ which is proportional to the second harmonic field amplitude that has been adiabatically eliminated. This is illustrated in the bottom panels of 8.

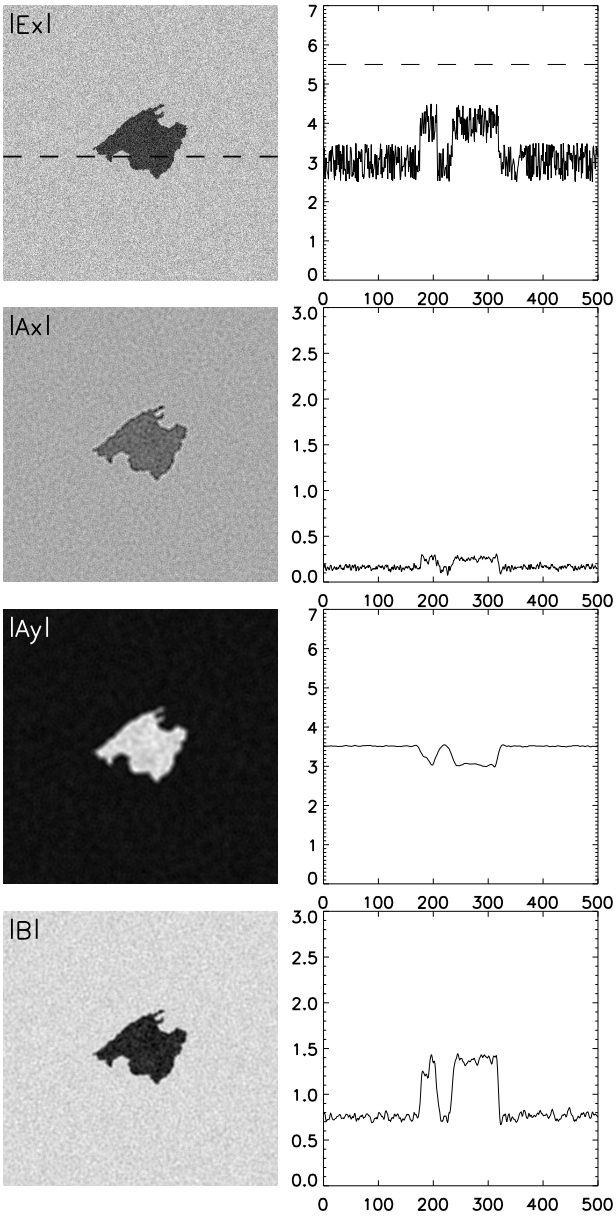

Fig. 6 Noise filtering in the frequency transfer regime. The left column shows (from top to bottom) the spatial distribution of amplitude of the input image $|E_x|$, and the amplitude of the intracavity fields $|A_x|$, $|A_y|$ and $|B|$. The gray scale of goes from the minimum (white) to the maximum (black) of each field. The right column shows a transversal cut of the fields. We have considered $|E_y| = 5$.

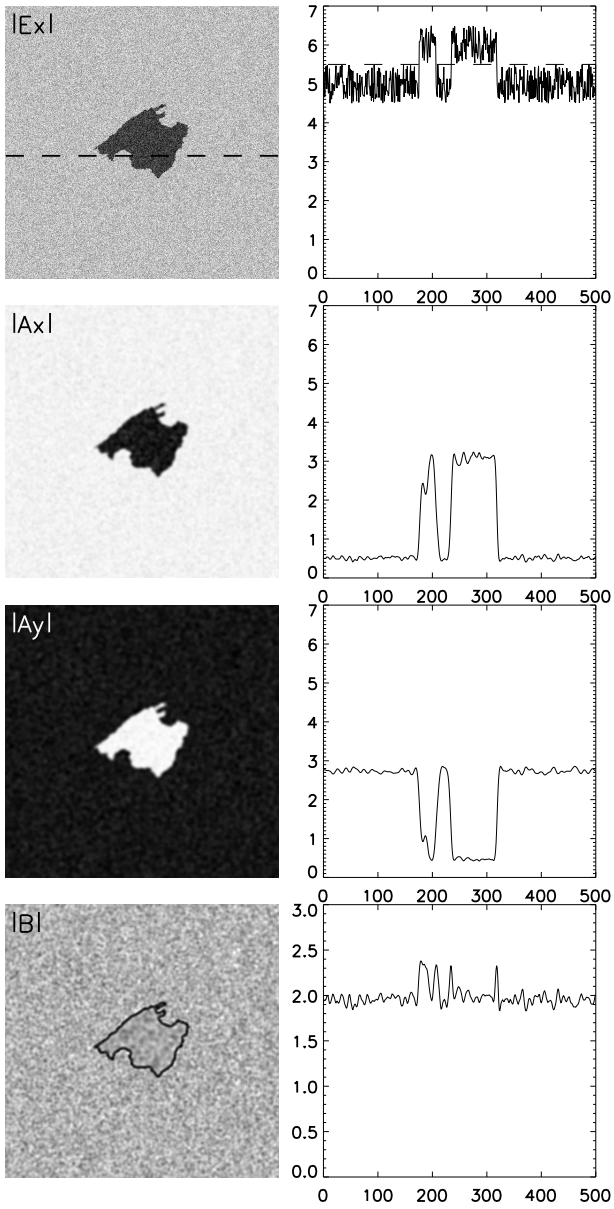

Fig. 7 Noise filtering in the contrast enhancement regime. The left column shows (from top to bottom) the spatial distribution of amplitude of the input image $|E_x|$, and the amplitude of the intracavity fields $|A_x|$, $|A_y|$ and $|B|$. The gray scale of goes from the minimum (white) to the maximum (black) of each field. The right column shows a transversal cut of the fields. We have considered $|E_y| = 5.5$.

5 Cavities with spherical mirrors

The previous section dealt with the ideal case of a cavity with plane mirrors whose realization is a nontrivial experimental challenge. Cavities with spherical mirrors are more stable and a more common experimental framework. We consider here a model for a cavity with spherical mirrors in quasi-confocal configuration. From a fundamental point of view, the introduction of curved mirrors breaks the translational invariance, which is an inconvenient for the processing of an image. Spatial points of the image where the field takes the same value and which would otherwise be treated in the same way are now treated differently if they are located at different distances from the optical axis.

To describe this system we use the full set of Eqs.3-5. In particular we consider a cavity characterized by the following parameters: $\delta = 1$, $\delta_0 = 0$, $\xi = 0.005$, $w_A^2 = 1$ and $w_B^2 = 0.5$ which correspond to a quasi-confocal configuration [10]. Due to the geometry of the cavity the pump fields have to decay to zero when $r \to \infty$. We

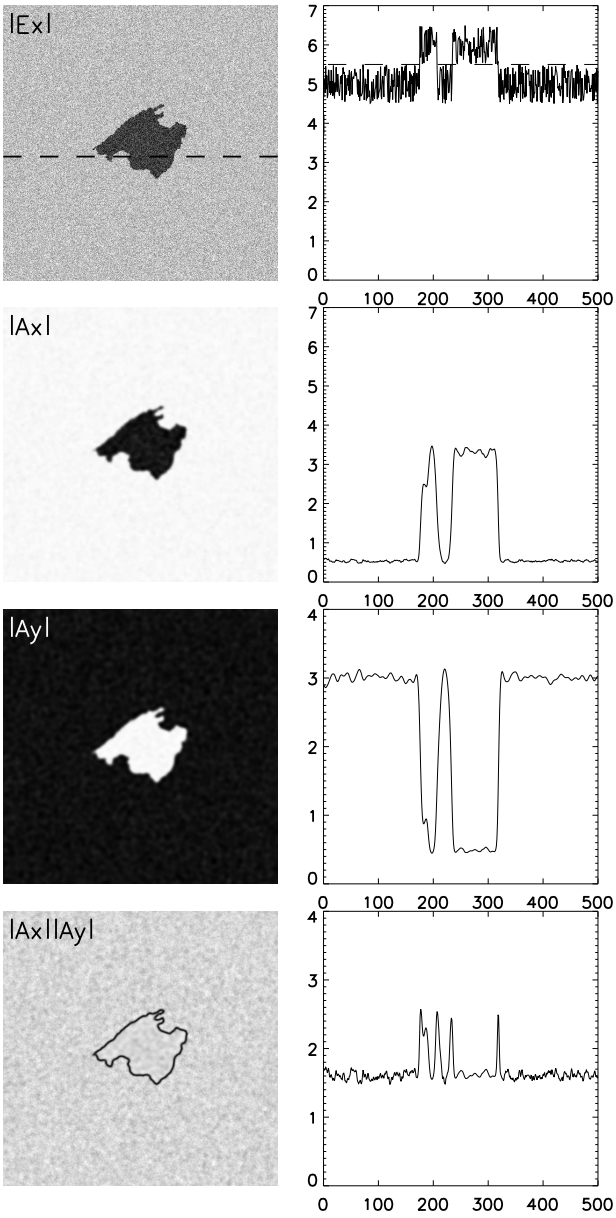

Fig. 8 Contrast enhancement and contour recognition in a single resonant planar cavity. The left column shows (from top to bottom) the spatial distribution of amplitude of the input image $|E_x|$, and the amplitude of the intracavity fields $|A_x|$, $|A_y|$ and the product $|A_x||A_y|$. The gray scale of goes from the minimum (white) to the maximum (black) of each field. The right column shows a transversal cut of the fields. We have considered $|E_y| = 5.5$.

consider a super-Gaussian holding beam which has a large plateau around the optical axis where we can superimpose the image. The input fields are: $E_y(r,\phi) = E_{0y}exp(-r^4/w_e^2)$, and $E_x(r,\phi) = I(r,\phi)+E_{0x}exp(-r^4/w_e^2)$, where $w_e = 300$ and $I(r,\phi)$ is an image as it has been considered in the planar cavity case. The input intensity levels are chosen such that they correspond to a regime where nonlinear effects are important.

While the simple geometrical construction used in section 5 can not be directly applied here, since there are no homogeneous steady state solutions, we found numerically that the amplitude of the y-polarized super-Gaussian beam plays again the role of setting a reference level. If the amplitude of the x-polarized image do not cross the amplitude of the y-polarized beam, then a (weak) image is transferred to the y-polarized second harmonic. This corresponds to the frequency transfer regime.

If a part of the image field crosses the value of the reference beam then contrast enhancement operation over that part of the image takes place as before. This is illustrated in Fig. 9. The upper panels show an x-polarized input field for a 2d image inserted on top of a super-Gaussian holding beam with $E_{0x} = 5$. The y-polarized reference beam is taken as a super-Gaussian with $E_{0y} = 5.5$. For all spatial points the image is above the reference level. The middle panels show the x-polarized intracavity field. The contrast of the image is clearly enhanced. Therefore the same contrast-enhancement operation obtained with planar cavities can be performed in cavities with spherical mirrors. The fact that the image is inserted on top of a super-Gaussian holding beam does not preclude any of the nonlinear operations since the reference beam is also a super-Gaussian. What really matters is the fact that locally the amplitude of the image superimposed to the holding beam crosses the amplitude reference beam. The main restriction comes from the fact that to achieve nonlinear effects the image should be placed on the central part or the beam where the input fields are strong enough.

Contour recognition operations can also be performed as before. As shown in fig. 10, the second harmonic field displays the contour of the image. Although now this contour is on top of a super-Gaussian beam, it is still clearly distinguishable.

Noise filtering effects do exist in cavities with spherical mirrors but the effect is smaller than in the planar cavity because the coefficient of the Laplacian term in 2, which takes into account diffraction, depends on the minimum waist of the intracavity fields. For the configuration considered here this coefficient takes a lower value than in the planar mirror case.

6 Summary

We have shown that intracavity second harmonic generation can be used for all-optical image processing. Operating in a linear regime it is possible to transfer an image from the fundamental to the second harmonic frequency. More important, by taking advantage of the system bistability it is possible to magnify the contrast in the fundamental field of any part of the image whose intensity is above a given reference level while simultaneously the second harmonic field displays the contour

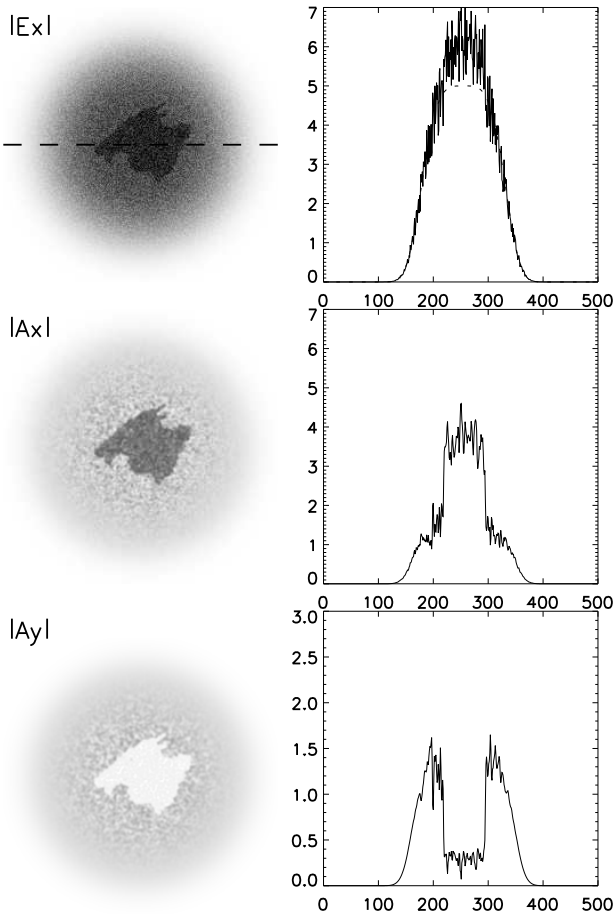

Fig. 9 Contrast enhancement in a quasi-confocal cavity. The left column shows (from top to bottom) the spatial distribution of amplitude of the input image $|E_x|$, and the amplitude of the intracavity fields $|A_x|$, $|A_y|$ and $|B|$. For each field the gray scale goes from zero (white) to the field maximum (black). In the right column a transversal cut of the fields is shown. The dashed line on the top right panel shows the profile of $|E_y|$

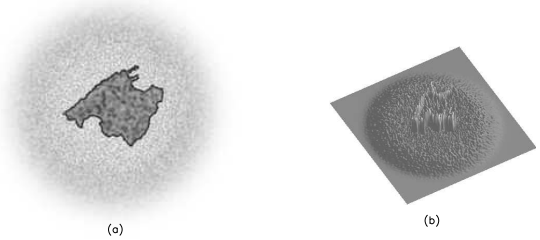

Fig. 10 Contour recognition in a quasi-confocal cavity for the image shown in the first row of Fig.9. The amplitude of the second harmonic field $|B|$ is shown as a gray scale on the left panel and as a 3d plot on the right panel. The gray scale goes from zero to the maximum of $|B|$.

of the same part of the figure. Furthermore, the reference level can be tuned allowing for a complete scan of the image and the cavity acts as a noise filtering device. This can be done using planar cavities both in the case where all the fields are resonant an in the case where only the fundamental harmonics are resonant as well as in the more common situation of cavities with spherical mirrors.

7 Acknowledgements

We acknowledge financial support from MEC (Spain) and FEDER under projects FIS2004-00953 (Conoce2), BFM2001-0341-C02-02 (Sinfibio) and BFM2001-4180-E. AJ acknowledges a PhD fellowship from MEC (Spain).

References

1. J. Teuber, Digital Image Processing, Prentice Hall, 1993.
2. J. Mitwinter and J. Warner, J. Appl. Phys. **38** (1967) 519
3. J. Mitwinter, Appl. Phys. Lett. **12** (1968) 68
4. F. Devaux, A. Mosset, E. Lantz, S. Monneret and H. Le Gall, Appl. Opt. **40** (2001) 4957
5. A.H. Firester, J. Appl. Opt. **40**, 4842 (1969); 4849 (1969)
6. F. Devaux and E. Lantz, J. Opt. Soc. Am. B **12** (1995) 2245
7. E. Lantz and F. Devaux, Quantum Semiclass. Opt. **9** (1997) 279
8. F. Devaux and E. Lantz, Opt. Commun. **114** (1995) 295
9. P. Scotto, P. Colet, M. San Miguel, Optics Letters **28**(2003) 1695-1679.
10. M.Marte, H. Ritsch, K.I. Petsas, A. Gatti, L. A. Luigiato, C.Fabre, D. Leduc, Optics Express **3** (1998) 71-79
11. P.Lodahl, M.Saffman, Phys. Rev. A,**60** (1999) 3251
12. U.Peschel, C. Etrich, F.Lederer, Opt. Lett, **23**, (1998) 500
13. U.Peschel, C. Etrich, F.Lederer, Phys. Rev E, **58**, (1998) 4005
14. S. Longhi, Opt. Lett, **23**, (1998) 346
15. S. Longhi, Phys. Rev. A, **59**, (1999) 346
16. Z. Y. Ou, Phys. Rev. A. **59**, (1999) 4021